J Neurophysiol 99: 2320–2328, 2008.
First published February 27, 2008; doi:10.1152/jn.00280.2007.

A Cost–Benefit Analysis of Neuronal Morphology

Quan Wen[1,2] and Dmitri B. Chklovskii[1]

[1]*Cold Spring Harbor Laboratory, Cold Spring Harbor; and* [2]*Department of Physics and Astronomy, State University of New York at Stony Brook, Stony Brook, New York*

Submitted 12 March 2007; accepted in final form 24 February 2008

Wen Q, Chklovskii DB. A cost–benefit analysis of neuronal morphology. *J Neurophysiol* 99: 2320–2328, 2008. First published February 27, 2008; doi:10.1152/jn.00280.2007. Over hundreds of millions of years, evolution has optimized brain design to maximize its functionality while minimizing costs associated with building and maintenance. This observation suggests that one can use optimization theory to rationalize various features of brain design. Here, we attempt to explain the dimensions and branching structure of dendritic arbors by minimizing dendritic cost for given potential synaptic connectivity. Assuming only that dendritic cost increases with total dendritic length and path length from synapses to soma, we find that branching, planar, and compact dendritic arbors, such as those belonging to Purkinje cells in the cerebellum, are optimal. The theory predicts that adjacent Purkinje dendritic arbors should spatially segregate. In addition, we propose two explicit cost function expressions, falsifiable by measuring dendritic caliber near bifurcations.

INTRODUCTION

Structure–function relationships have long played an important role in biology. In addition to describing the bewildering variety of axonal and dendritic arbor shapes, Cajal has inferred that the function of dendrites and axons was to conduct signals from postsynaptic terminals to the integration site, which often is the cell body, and from the integration site to the presynaptic terminals, respectively (Ramón y Cajal 1899). Moreover, he speculated qualitatively that the structure of axons and dendrites minimizes their cost for given functional constraints (Ramón y Cajal 1899). Nonetheless, a quantitative theory of axonal and dendritic shape and dimensions, which could provide valuable insights into their function, is still missing (Cline 2001; Fiala and Harris 1999; Jan and Jan 2003; Scott and Luo 2001; Whitford et al. 2002; Wittenberg and Wang 2007).

In some cases, axonal dimensions can be trivially explained by the requirement of making specific connections. In particular, global axons projecting over long distances must be long enough to reach from the presynaptic cell body to the postsynaptic target(s). For example, an axon of a pyramidal neuron projecting from one cortical area to another must be as long as the distance between those areas. Even local axons sometimes make specific connections that determine their shape. For example, the shape of climbing fiber in the cerebellum and ascending branches of granule cell axons must match the shape of Purkinje cell dendrites so that the axonal arbor can make numerous contacts with a single dendrite (Llinás et al. 2004). Most dendrites do not implement long-range projections (gustatory neurons being a major exception), yet they may have specific local targets. For example, apical dendrites of many pyramidal neurons arborize only in certain cortical layers.

In many cases, however, the requirement to make specific connections does not fully determine arbor dimensions. Consider, for example, Purkinje cell dendrites, which can establish a synapse by just growing a spine with most parallel fibers (major part of granule cell axons) that course through their dendritic volume. There is no specificity in the topology and dimensions of the dendritic arbor. What determines the topology and dimensions of these dendrites?

Dendrites are just long enough to accommodate a given number of potential synapses (Chklovskii 2004). We define *potential synapse* as a location where an axon passes within a spine length of a dendrite (Fig. 1*A* and Stepanyants et al. 2002). A potential synapse can convert into actual just by growing a spine (Trachtenberg et al. 2002). Due to volume exclusion by axons forming potential synapses, the dendritic length is approximately equal to the number of such axons times the axonal cross-sectional area divided by the spine length (Fig. 1*A*).

The preceding argument accounts for the total length of dendrites and axons but does not explain why dendrites and axons branch. For example, let us consider two alternative designs for a dendritic arbor [Fig. 2, *A* and *B* modified from Murre and Sturdy (1995)]. For simplicity, we assume that these arbors are planar and they must receive inputs from a bundle of axons running perpendicular to the dendritic plane, just like parallel fibers in the cerebellum. Both arbors have the same total length and the same number of potential axons. Therefore their total wire length cost and potential connectivity are the same. Why does not the arbor in Fig. 2*B* exist in the brain?

One possible answer is that branching plays a computational role in axons (Debanne 2004; Grossman et al. 1979a,b; Manor et al. 1991) and, in particular, dendrites (Agmon-Snir et al. 1998; Koch 1999; London and Häusser 2005; Mainen and Sejnowski 1996). For example, interactions between excitatory and inhibitory inputs on different dendritic branches may be used to construct logical gates (Koch et al. 1982). A large number of dendritic branches may also increase the information storage capacity of a neuron because synaptic inputs from different branching units may combine nonlinearly (Poirazi and Mel 2001). However, a quantitative theory of dendritic branching based on computational requirements does not exist.

In this work, we sought to rationalize the branching structure of dendrites by minimizing the dendritic cost, which increases with not only the total dendritic length, but also the path length from synapses to soma (Cuntz et al. 2007; Wen and Chklovskii

Address for reprint requests and other correspondence: D. B. Chklovskii, Janelia Farm Research Campus, Howard Hughes Medical Institute, 19700 Helix Drive, Ashburn VA 20147 (E-mail: chklovskiid@janelia.hhmi.org).

The costs of publication of this article were defrayed in part by the payment of page charges. The article must therefore be hereby marked "*advertisement*" in accordance with 18 U.S.C. Section 1734 solely to indicate this fact.

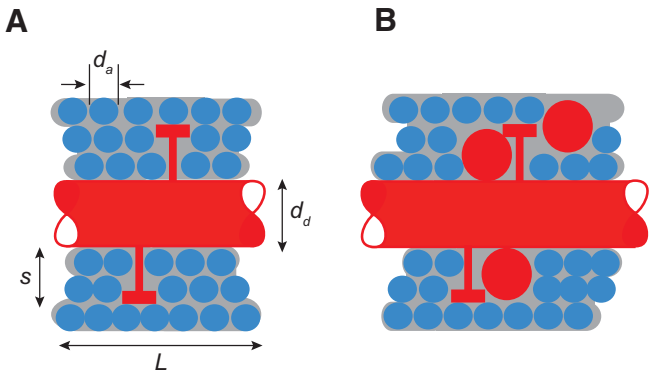

FIG. 1. Schematic illustration of two designs of the neuropil microarchitecture near a dendrite. Axons (blue) make potential synapses with a dendritic segment (red) if they pass through a region within a spine length s of that segment. We call this region a spine-reach zone and compare two designs with the same number of potential synapses. *A*: spine-reach zone contains axons but excludes dendrites of other neurons. d_a, axon diameter; d_d, dendritic diameter; L, dendritic length. *B*: dendrites from various neurons interpenetrate each other's spine-reach zone. As a result, they add to the excluded volume of axons and increase the total length of dendrites L.

2005). The motivation for such an approach is that longer path length leads to longer time delays (Chklovskii et al. 2002; Wen and Chklovskii 2005), greater attenuation of synaptic signals (Zador et al. 1995), and higher metabolic costs for intracellular transport (Burke et al. 1992). We minimize dendritic cost for a fixed number of axons establishing potential synapses with a dendritic arbor.

In the first-order approximation, the shape of a dendritic arbor is determined by the axonal class that provides numerically dominant input to the dendrites. In the case of Purkinje cell dendrites, the majority of synapses are formed by parallel fibers, whereas interneuron axons, climbing fibers, and ascending branches of granule cell axons contribute only a minority of synaptic inputs. Thus we consider the impact of only parallel fiber input on the shape of Purkinje cell dendrites.

The paper is organized as follows. First, assuming only that dendritic cost increases with total dendritic length and path length from synapses to soma, we find that optimal dendritic arbors should be branching, compact, and planar (perpendicular to the orientation of axons). In addition, dendritic arbors should avoid overlap of spine-reach zones. Second, we demonstrate that Purkinje cell dendrites in the cerebellum are consistent with such design. Third, we propose two detailed models of dendritic cost that yield different predictions for the changes of the dendritic diameter across bifurcations and thus can be tested experimentally. Although for the sake of concreteness we consider dendritic arbors, our reasoning should apply to axonal arbors as well. A preliminary account of this work was presented at the 2005 annual meeting of the Society for Neuroscience in Washington DC.

METHODS

Calculation of the mesh size of Purkinje dendritic arbors

To measure the mesh size of a dendritic arbor, first, we projected the cells onto the plane perpendicular to the parallel fibers (sagittal plane). Second, we drew circles intersecting the arbor and calculated the mesh size by dividing the area of the circle by the total dendritic length within the circle (Fig. 4). We repeated the procedure by using different dendritic segments as centers and different circle radii r (Fig. 4). Because circles near the exterior boundary of the arbor intersect fewer branches than they normally do, we restricted our measurement to the interior part of the arbor by requiring that the distance between the center of a circle and the centroid of the arbor is less than the gyration radius of the arbor R_g. The gyration radius of the arbor is defined as $R_g = (1/N)\sum_{i=1}^{N} |\mathbf{r_i} - \mathbf{r_c}|^2$, where $\mathbf{r_i}$ and $\mathbf{r_c}$ are Cartesian coordinates of a dendritic segment and the centroid of the arbor, respectively. Third, the mean mesh size, which was obtained by averaging over different centers of the circles and different cells, was plotted as a function of r^2 normalized by R_g^2.

Derivation of the branching law by minimization of the dendritic surface area and signal attenuation cost

To derive the branching law from minimization of surface area and attenuation, we write the cost function (*Eq. 30*) for a bifurcation consisting of three segments with unit length (Fig. 6)

$$E_{bp} = d_1 + c_1\alpha\frac{1}{\beta d_1^{1/2}} + d_2 + c_2\alpha\frac{1}{\beta d_2^{1/2}} + d_0 + (c_1 + c_2)\alpha\frac{1}{\beta d_0^{1/2}} \quad (1)$$

In *Eq. 1* we have used the space constant $\lambda = \beta d_d^{1/2}$, where β is a proportionality constant depending on the specific membrane resis-

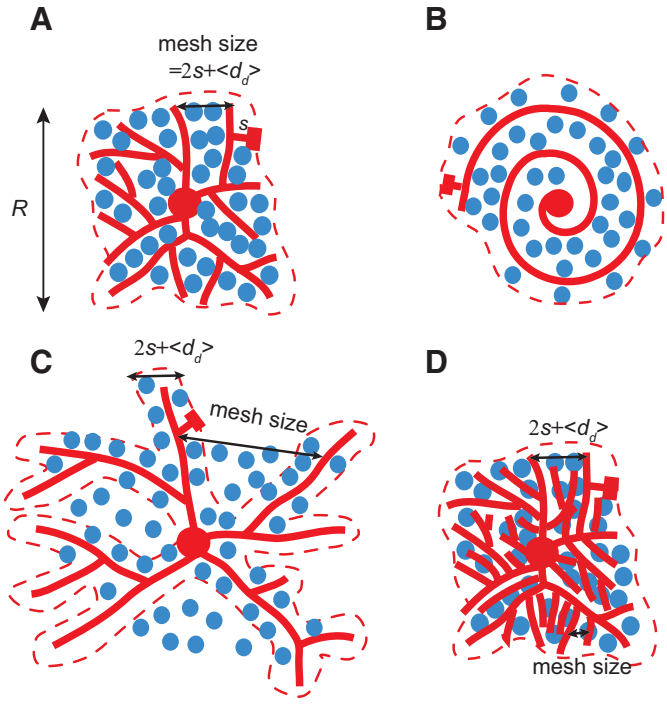

FIG. 2. Schematic illustration of four dendritic arbor designs. Dendrites (red) could be either planar or 2-dimensional (2D) projections of 3-dimensional (3D) arbors onto the plane perpendicular to axons (blue). We consider four designs with the same number of potential axonal targets. Dashed line indicates the spine-reach zone of an arbor. s, spine length; $\langle d_d \rangle$, mean dendritic diameter; R, arbor span. *A*: a compact branching arbor makes on average one potential synapse with each axon (blue) passing through the arbor. The mesh size, defined as the arbor area divided by the total dendritic length, is $2s + \langle d_d \rangle$ for a compact planar arbor and is the same, up to a numerical factor of order one, for a compact 3D arbor. *B*: a compact nonbranching arbor has the same total dendritic length and mesh size as those of the compact branching arbor but greater path length. *C*: a sparse branching arbor does not make potential synapse with every axon passing through arborist territory because the area of the spine-reach zone is smaller than the arbor area. The mesh size of a sparse arbor is much larger than $2s + \langle d_d \rangle$. *D*: a dense branching arbor makes more than one potential synapse with each axon passing through arborist territory. The mesh size of a dense arbor is much smaller than $2s + \langle d_d \rangle$.

tance and the intracellular resistivity, whereas c_1 and c_2 are proportional to the number of synapses on the trees stemming from the two daughter branches.

By setting $\partial E_{bp}/\partial d_1 = 0$, $\partial E_{bp}/\partial d_2 = 0$, and $\partial E_{bp}/\partial d_0 = 0$, we obtain the optimal diameters

$$d_1 = \left(\frac{c_1\alpha}{2\beta}\right)^{2/3} \quad d_2 = \left(\frac{c_2\alpha}{2\beta}\right)^{2/3} \quad d_0 = \left(\frac{c_1 + c_2}{2\beta}\alpha\right)^{2/3} \tag{2}$$

It is easy to see that these diameters obey the relationship $d_0^{3/2} = d_1^{3/2} + d_2^{3/2}$.

Note that to find the optimal dendritic diameters in *Eq. 1*, we assume that the number of synapses along a dendritic branch does not depend on the dendritic diameter. Because the path length of a branch in a compact dendritic arbor is a function of $\langle d_d\rangle/2s$ (*Eq. 15*), our derivation is justified if $\langle d_d\rangle \ll 2s$, so that the impact of the variations of dendritic diameters on the spatial distribution of synapses on an arbor can be ignored.

RESULTS

Dendritic cost function and potential connectivity constraints

We start by considering the properties of the dendritic cost function. Based on the observation that arbor volume and path length invoke costs, we assume that dendritic cost E grows with the total dendritic length L, i.e., $\partial E/\partial L > 0$, and with the average path length from a synapse to the soma ℓ, i.e., $\partial E/\partial \ell > 0$ for all L and ℓ. These rather general assumptions will be sufficient to make predictions about optimal dendritic shape. Under DISCUSSION we will formulate two concrete models that satisfy the preceding assumptions.

Next, we switch our attention to the constraints. Requiring a potential convergence factor imposes the following constraints on L and ℓ. For simplicity, let us first consider a planar dendritic arbor and axons running orthogonally to it. C axons must fit within a spine length s of a dendrite, which we call the *spine-reach zone*. Then, the area of the spine-reach zone ($2sL$) must be at least equal to the total cross-sectional area of the axons ($\pi/4Cd_a^2$) (Fig. 1). Therefore we have the following inequality constraint for L

$$L \geq \frac{\pi}{4}Cd_a^2/2s \tag{3}$$

Because the mean path length ℓ can only be greater than or on the same order of linear arbor span R, we obtain

$$\ell \geq \eta R \tag{4}$$

where η is a numerical factor of order one. For a planar arbor, the arbor span area A must satisfy

$$A \geq \frac{\pi}{4}Cd_a^2 + \langle d_d\rangle L \tag{5}$$

where $\langle d_d\rangle$ is the mean dendritic diameter and $\langle d_d\rangle L$ is the area occupied by the dendrite on the plane. By substituting *Eq. 3* into *Eq. 5*, we have

$$A \geq \frac{\pi}{4}Cd_a^2(1 + \langle d_d\rangle/2s) \tag{6}$$

For circular arbors, we have $R \approx 2(A/\pi)^{1/2}$. Then combining the inequalities in *Eqs. 4* and *6* yields the inequality constraint for ℓ

$$\ell \geq \eta C^{1/2}d_a(1 + \langle d_d\rangle/2s)^{1/2} \tag{7}$$

Optimal dendritic arbor is planar, compact, and centripetal

In this section, we minimize the cost function E subject to the constraints given by *Eqs. 3* and *7*. First, we convert the inequality constraints into equality constraints by adding two slack variables, z_1^2 and z_2^2

$$L = \frac{\pi}{4}Cd_a^2/2s + z_1^2 \tag{8}$$

$$\ell = \eta C^{1/2}d_a(1 + \langle d_d\rangle/2s)^{1/2} + z_2^2 \tag{9}$$

Next, we transform our constrained optimization problem into an unconstrained optimization problem by using Lagrange multipliers

$$\mathcal{L} = E + \lambda_1\left(\frac{\pi}{4}Cd_a^2/2s - L + z_1^2\right) + \lambda_2[\eta C^{1/2}d_a(1 + \langle d_d\rangle/2s)^{1/2} - \ell + z_2^2] \tag{10}$$

To find the minimum, we require

$$\frac{\partial\mathcal{L}}{\partial L}=0 \quad \frac{\partial\mathcal{L}}{\partial \ell}=0 \quad \frac{\partial\mathcal{L}}{\partial z_1}=0 \quad \frac{\partial\mathcal{L}}{\partial z_2}=0 \quad \frac{\partial\mathcal{L}}{\partial \lambda_1}=0 \quad \frac{\partial\mathcal{L}}{\partial \lambda_2}=0 \tag{11}$$

From the first two conditions, we obtain

$$\frac{\partial E}{\partial L} - \lambda_1 = 0 \quad \frac{\partial E}{\partial \ell} - \lambda_2 = 0 \tag{12}$$

The third and the forth conditions yield

$$2\lambda_1 z_1 = 0 \quad 2\lambda_2 z_2 = 0 \tag{13}$$

Assuming $\partial E/\partial L > 0$ and $\partial E/\partial \ell > 0$, the preceding conditions are satisfied only if $\lambda_1 > 0$, $\lambda_2 > 0$, and $z_1 = z_2 = 0$. Thus both constraints become active

$$L = \frac{\pi}{4}Cd_a^2/2s \tag{14}$$

$$\ell = \eta C^{1/2}d_a(1 + \langle d_d\rangle/2s)^{1/2} \tag{15}$$

If *Eq. 15* holds, the inequalities of *Eqs. 4* and *6* become equalities

$$\ell = \eta R \tag{16}$$

$$A = \frac{\pi}{4}Cd_a^2(1 + \langle d_d\rangle/2s) \tag{17}$$

Dendritic arbors satisfying *Eqs. 14–17* have the following properties. First, minimizing total dendritic length (*Eq. 14*) demands a spatial organization of the neuropil, in which adjacent dendrites from different neurons are excluded from each other's spine-reach zone (Fig. 1*A*). If dendrites penetrated each other's spine-reach zones (Fig. 1*B*), they would add to the excluded volume of axons and would increase the total dendritic length.

Second, to achieve the minimum path length ℓ in *Eq. 15*, each segment of the dendrite should be directed toward the soma. We call such arbor design centripetal. If the total dendritic length is greater than the dendritic arbor span, the centripetal arbor must branch (Fig. 2*A*). Therefore branching of dendrites is a trivial consequence of minimizing the mean path length.

In suboptimal dendritic arbors, the dependence of ℓ on R does not have to be linear, as suggested by *Eq. 16* (Fig. 3*A*). For example, if dendrites consisted of randomly oriented segments, as in a random walk (Fig. 3*B*), the path length would be $\ell \sim R^2$.

Third, we calculate the arbor mesh size—a parameter that quantifies the sparseness of an arbor—by dividing the arbor area by the total length, A/L. By combining *Eqs. 14* and *17*, we find that

$$\frac{A}{L} = 2s + \langle d_d \rangle \tag{18}$$

We call an arbor satisfying *Eq. 18* compact (Fig. 2*A*). One property of a compact arbor is that it forms on average one potential synapse with each axon passing through the arbor.

A compact branching arbor is less costly than other branching arbors with the same potential convergence. Consider a sparse arbor, the mesh size in which is much larger than $2s + \langle d_d \rangle$ (Fig. 2*C*), and which does not form potential synapses with every axon passing through the arbor (Fig. 2*C*). A compact arbor is less costly because it has a smaller span than that of a sparse branching arbor. A compact branching arbor is also advantageous to a dense branching arbor, in which the arbor mesh size is much smaller than $2s + \langle d_d \rangle$ (Fig. 2*D*). A dense branching arbor can form more than one potential synapse with each axon passing through the arbor (Fig. 2*D*). Given the same number of axons forming potential synapses with the dendrite, such design makes the total dendritic length greater than that in the compact arbor.

How does this analysis of a planar dendritic arbor generalize to three-dimensional (3D) dendritic arbors? When axons run in different directions and the arbor is 3D, the above-cited results still hold if numerical factors of order one are ignored. Yet when these numerical factors are included, a planar arbor is preferable. A planar arbor can be viewed as a two-dimensional (2D) projection of a 3D arbor and the projection is always shorter than the original. Thus both the minimum path length (ℓ) and the minimum total dendritic length (L) in a planar arbor are shorter than those in a 3D arbor.

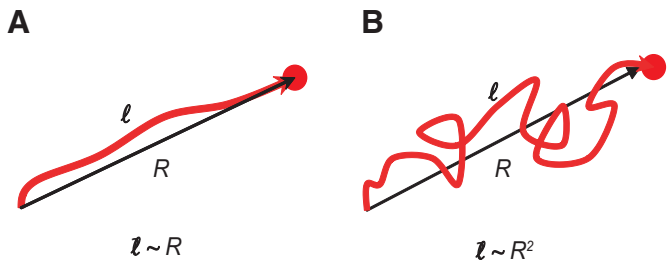

FIG. 3. Dependence of the path length on the arbor span. *A*: in the optimal dendritic arbor, dendritic branches are fully stretched so that the path length from a dendritic site to the soma is on the same order as the arbor span. *B*: in a hypothetical dendritic arbor defined by a random-walk trajectory, orientations of dendritic segments are statistically independent and $\ell \sim R^2$.

Purkinje dendritic arbors are planar, compact, and centripetal

In the previous section, we derived the properties of optimal dendritic arbors that minimize cost for given potential connectivity. Next, we compare our predictions with the experimental measurements for Purkinje dendritic arbors. Because Purkinje arbors are evidently planar, we demonstrate that they are compact and centripetal.

To prove that Purkinje dendritic arbors are compact, we refer to *Eq. 18* and show that the mesh size of a dendritic arbor is $2s + \langle d_d \rangle$. Napper and Harvey (1988b) reported that $s = 1.4$ μm, as measured from the surface of the dendrites to the tip of the spine. They also found the diameter of spiny dendrites receiving parallel fiber inputs to be $\langle d_d \rangle = 1.5$ μm. This yields the mesh size of 4.3 μm (red line in Fig. 4*B*), reasonably close to the direct measurements, obtained by dividing the area of a part of an arbor by the dendritic length of that part (see METHODS and Fig. 4 for details).

To demonstrate that Purkinje cell dendrites are centripetal, we calculated the distribution of dendritic segments' orientation angles θ (Fig. 5*A*), where θ is defined as the angle between the vector of the signal flowing along a dendritic segment and the vector pointing centripetally from the segment to the soma. Figure 5*B* shows a Purkinje dendritic arbor where each dendritic segment is colored according to the value of θ. We found that 70% of the segments have orientation angles $<90°$ (Fig. 5*A*), which suggests that Purkinje dendritic segments are predominately centripetal. This observation is consistent with the measurements of pyramidal cell dendrites in hippocampus (Samsonovich and Ascoli 2003).

Many trajectories observed in nature are not centripetal and one of the classical examples is a random walk. For comparison, we simulated a random walk consisting of rigid segments 5 μm in length with random orientations and plotted the probability distribution of orientation angles (gray line in Fig. 5*A*). In a 3D random walk, the most likely orientation angle is near 90° (Fig. 5*A*).

In optimal dendrites, the typical path length from a dendritic segment to the soma must be on the order of the Euclidean distance between them (*Eq. 16*), i.e., the tortuosity index, defined as the ratio of the path length from a dendritic segment to the soma to the Euclidean distance between the two locations, is of order one. To verify that dendrites are optimal, we plot the tortuosity in Purkinje cell dendrites as a function of path length (Fig. 5*C*). Unlike the simulated dendrites with random-walk trajectories, the tortuosity of real dendrites is close to one (Fig. 5*C*), consistent with optimality.

Microarchitecture of the cerebellum molecular layer

To verify that Purkinje cell dendrites from different neurons are excluded from each other's spine-reach zone (Fig. 1*A*), we shall estimate the interval b between potential synapses along a parallel fiber in the molecular layer and show that $b = 2s + \langle d_d \rangle$ (Napper and Harvey 1988a).

The interval between potential synapses along a parallel fiber $b = L_a/D$, where L_a is the length of a parallel fiber and D is the potential divergence factor. D can be calculated as follows. Because Purkinje cell dendrites are compact, an axon can potentially connect with all the dendrites in the volume

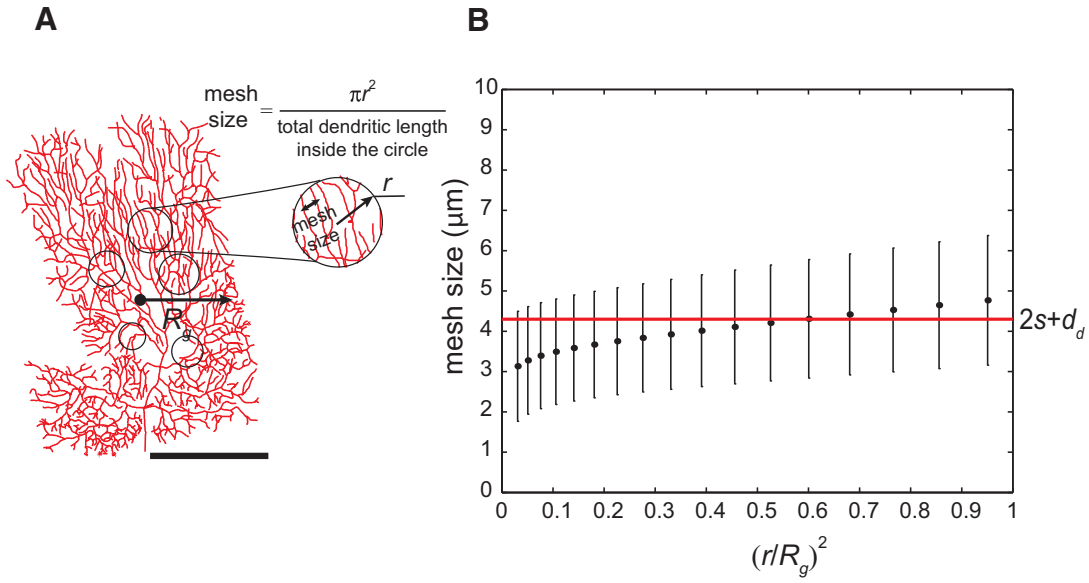

FIG. 4. Purkinje dendritic arbors are compact. Arbor mesh size of Purkinje cell dendrites. *A*: to measure the mesh size, we divided the area of arbitrarily drawn circles by the total dendritic length inside the circles. Scale bar: 50 and 10 μm in the enlargement. *B*: the mean mesh size averaged over different circle positions and different cells as a function of the normalized area of the circle (see METHODS for detailed description). The total number of observations per point is 17,508. The red line corresponds to the mesh size predicted for a compact arbor, $2s + \langle d_d \rangle$, using $s = 1.4$ μm and $\langle d_d \rangle = 1.5$ μm (Napper and Harvey 1988b). Error bars are SDs. The preceding analysis was done on 10 digitally reconstructed Purkinje dendritic arbors (Martone et al. 2003; Rapp et al. 1994; Vetter et al. 2001) available from http://neuromorpho.org.

$L_a wh$, where w is the width of the dendritic arbor and h is the height of the arbor. Therefore we have

$$D = \rho L_a wh \tag{19}$$

where ρ is the neuronal density. Because Purkinje cell bodies are arranged uniformly in a layer, we may rewrite *Eq. 19* as a function of the neuronal density per unit area σ

$$D = \sigma L_a w \tag{20}$$

As a result, the interval of potential synapses on an axon b is given by

$$b = L_a/D = \frac{1}{\sigma w} \tag{21}$$

By substituting the values from the rat cerebellum (Napper and Harvey 1988a) $\sigma = 1{,}018$ mm^{-2}, $w = 250$ μm, we obtain $b = 4$ μm. Recalling that $s = 1.4$ μm, $d_d = 1.5$ μm (Napper and Harvey 1988b), we find that the relation $b = 2s + d_d$ is satisfied and adjacent Purkinje cell dendrites are on average excluded from each other's spine-reach zone. We hope that in the future this calculation will be verified directly by electron microscopic reconstructions.

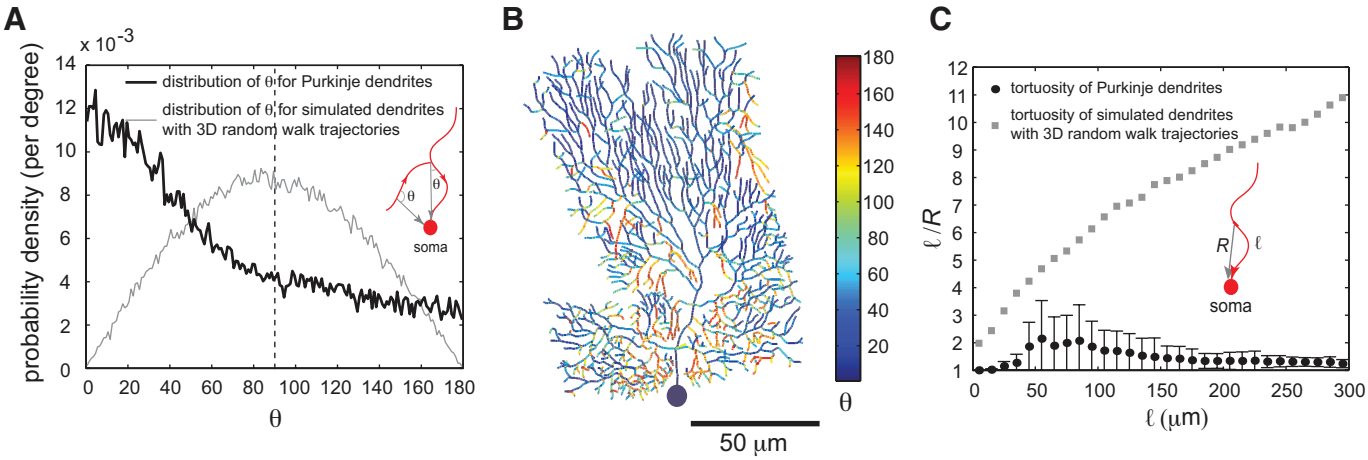

FIG. 5. Purkinje dendritic arbors are centripetal. *A*: the probability distribution of the orientation angle θ between the vector associated with a Purkinje dendritic segment and the vector pointing centripetally from the segment to the soma (black line). Some 70% of the segments have angles $<90°$ (the total area under the black curve from 0 to 90°). Gray line is the probability distribution of angles for dendritic branches generated by 3D random-walk trajectories. Random walk is not centripetal because the distribution has a peak near 90°. *B*: a digitized Purkinje dendritic arbor, where the color of each dendritic segment represents the value of the orientation angle. *C*: the tortuosity of Purkinje cel dendrites, which is defined as the ratio of the path length from the soma to a dendritic segment to the Euclidian distance between the 2 locations, is close to one for different path length from dendritic segments to the soma. The tortuosity of dendrites generated by random-walk trajectories is much higher than that of Purkinje cell dendrites and it scales with the square root of the path length. All error bars are SDs. The preceding analysis was done on 10 digitally reconstructed Purkinje dendritic arbors (Martone et al. 2003; Rapp et al. 1994; Vetter et al. 2001) available from http://neuromorpho.org. The arbors were projected onto the plane perpendicular to the parallel fibers (sagittal plane).

DISCUSSION

We rationalized compactness, branching, planarity, and mutual exclusivity of Purkinje cell dendrites while making only generic assumptions about dendritic cost function E ($\partial E/\partial L > 0$ and $\partial E/\partial \ell > 0$). Next, we propose two explicit expressions for the cost function based on detailed models. These cost functions satisfy our assumptions and make different predictions about the distribution of dendritic diameters along the arbor.

In both models, we propose that dendritic cost is quantified by the total area of the plasma membrane. The rationale comes from the observation that the energy to maintain the resting potential of a membrane is proportional to its surface area (Attwell and Laughlin 2001; Lennie 2003). To maintain a low [Na^+] inside a cell, sodium ions permeating into a neuron must be actively extruded by Na^+/K^+ pump. The number of ions extruded is proportional to the membrane conductance (Attwell and Laughlin 2001; Lennie 2003) and thus proportional to the membrane surface area

$$E \sim L\langle d_d \rangle \tag{22}$$

Here and below, we use symbol $\sim$ to indicate that numerical factors of order one are dropped or to reflect a scaling relationship.

Although dendritic cost decreases as the mean dendritic diameter $\langle d_d \rangle$ is reduced, a small diameter would detrimentally affect dendritic function for at least two reasons: transport of synaptic proteins (model 1) and attenuation of synaptic currents (model 2). In model 1, we assume that the transport of proteins from soma to synapses determines dendritic dimensions. In model 2, we assume that dendritic dimensions minimize the combination of surface area and signal attenuation from synapses to soma.

Model 1: minimization of dendritic surface area subject to transport constraint

We posit a transport model in which the number of synapses on a dendrite determines the rate of protein transport along that dendrite. Assuming that the rate of transport is proportional to the number of microtubules at a given cross section of a dendrite, the number of microtubules should be proportional to the number of synapses downstream of that cross section. If the density of microtubules (per cross-sectional area) is roughly invariant, the cross-sectional area must be proportional to the number of microtubules and thus to the number of synapses downstream. A similar argument has been made for axons (Hsu et al. 1998).

The preceding model predicts that the number of microtubules is conserved across a bifurcation. Assuming constant density of microtubules, dendritic diameters at a bifurcation point (Fig. 6) obey a quadratic branching law, as suggested previously (Hillman 1979; Wittenberg and Wang 2007): $d_0^2 = d_1^2 + d_2^2$, where d_0^2 is the cross-sectional area of the mother branch and d_1^2, d_2^2 are the cross-sectional areas of the daughter branches.

We next show how to estimate the average dendritic diameter $\langle d_d \rangle$ within our transport model. We subsequently assume that the total number of synapses on a dendritic arbor is proportional to the potential convergence factor C. Then, given

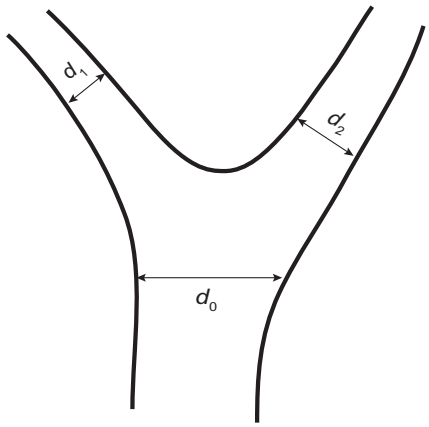

FIG. 6. Dendritic diameters at a bifurcation point. d_0 is the mother branch diameter and d_1, d_2 are daughter branch diameters.

the specified transport properties, the total dendritic volume V should scale as

$$V \sim C\ell \tag{23}$$

Since dendritic volume can be expressed in terms of the dendritic diameters and length

$$V = \langle d_d^2 \rangle L \tag{24}$$

$\langle d_d^2 \rangle$ can be expressed by ℓ and L as follows

$$\langle d_d^2 \rangle \sim C\ell/L \tag{25}$$

If the SD of dendritic diameters is smaller than the mean (Gundappa-Sulur et al. 1999; Rapp et al. 1994), we may approximate $\langle d_d^2 \rangle$ as $\langle d_d \rangle^2$. Then, by substituting *Eq. 25* into the expression for the total dendritic surface area, we find that

$$E \sim C^{1/2} L^{1/2} \ell^{1/2} \tag{26}$$

which is consistent with our assumptions about the cost function (i.e., $\partial E/\partial L > 0$ and $\partial E/\partial \ell > 0$). Thus the properties of optimal dendritic arbors derived in previous sections apply to this specific model.

In addition, if L is proportional to C and thus proportional to the number of synapses on a dendritic arbor (Purves 1988), dendritic diameters obey the following scaling relations. First, the sum of cross-sectional areas of stem segments near the soma should be proportional to L. Second, *Eq. 25* yields $\langle d_d^2 \rangle \sim \ell$. Third, in the limit $\langle d_d \rangle \ll 2s$, $\ell \sim C^{1/2}$ (*Eq. 15*), and thus we obtain $\langle d_d^2 \rangle \sim \ell \sim C^{1/2} \sim L^{1/2}$. The opposite limit is biologically irrelevant because no dendrites with $\langle d_d \rangle \gg 2s$ have been observed.

Model 2: minimization of dendritic surface area and signal attenuation cost

In the second model, we assume that the cost function is a sum of dendritic surface area and signal attenuation cost T

$$E = \langle d_d \rangle L + \alpha T \tag{27}$$

where α is an unknown constant, which will be determined later from the comparison with experimental data. We note that a similar form of the cost, which combines volume and time

delay, was previously applied to axons (Chklovskii and Stepanyants 2003).

Although the surface area of a dendritic arbor can be minimized by making dendrites thinner, such a design would negatively affect dendritic function: thinner dendrites substantially attenuate synaptic currents. Reduction of synaptic efficacy due to dendritic attenuation can be expressed in terms of the fractional dissipation of input charges from all the synapses to the soma

$$T \sim C(1 - Q_{soma}/Q_{syn}) \tag{28}$$

where Q_{syn} and Q_{soma} are the amount of charges delivered at a synaptic site and the soma, respectively.

According to the passive cable theory, the inward charge attenuation factor Q_{soma}/Q_{syn} is identical to the outward steady-state voltage attenuation factor (Koch 1999), which is defined as the voltage attenuation at a dendritic site when injecting a constant current in the soma. The attenuation factor can be approximated by $\exp(-\ell/\lambda)$ (Zador et al. 1995), where λ is the space constant and ℓ/λ is the electrotonic length.

Experimental measurements in Purkinje cell dendrites (Roth and Häusser 2001) and basal pyramidal dendrites (Nevian et al. 2007) suggest that $\ell \ll \lambda$. In this case, by expanding the $Q_{soma}/Q_{syn} = \exp(-\ell/\lambda)$ to the first order, *Eq. 28* becomes

$$T \sim C\ell/\lambda \tag{29}$$

As the space constant λ grows with dendritic diameter (Rall 1959), minimization of the attenuation cost favors a thicker dendritic diameter.

By combining *Eqs. 27* and *29*, we arrive at the expression for the dendritic cost

$$E = \langle d_d \rangle L + \alpha \frac{C\ell}{\lambda} \tag{30}$$

Equation 30 is consistent with our assumptions about the cost function (i.e., $\partial E/\partial L > 0$ and $\partial E/\partial \ell > 0$).

Minimization of the above-cited dendritic cost (*Eq. 30*) yields a branching law, $d_0^{3/2} = d_1^{3/2} + d_2^{3/2}$ (see Fig. 6 and METHODS), different from the one derived in the previous section. This relationship is mathematically identical to Rall's law derived from impedance matching considerations (Rall 1959).

Next, we estimate the average dendritic diameter $\langle d_d \rangle$. If we neglect variations in diameter of dendritic branches and express the space constant $\lambda = \beta \langle d_d \rangle^{1/2}$, then, by substituting the expressions for L and λ (*Eqs. 14* and *15*) into *Eq. 30*, we find

$$E \approx C\langle d_d \rangle \frac{d_a^2}{2s} + \alpha C^{3/2} d_a \frac{(1 + \langle d_d \rangle/2s)^{1/2}}{\beta \langle d_d \rangle^{1/2}} \tag{31}$$

By setting $\partial E/\partial \langle d_d \rangle = 0$, we obtain

$$\langle d_d \rangle^4 + 2s\langle d_d \rangle^3 \approx (\alpha/\beta)^2 2s^3 C/d_a^2 \tag{32}$$

An explicit expression for the optimal $\langle d_d \rangle$ can be found in the limiting cases. From *Eq. 32*, we obtain $\langle d_d \rangle \sim C^{1/3} \sim L^{1/3}$, provided that $\langle d_d \rangle \ll 2s$.

Finally, we may determine the unknown constant α in the cost function (*Eq. 27*) by substituting physiological and anatomical parameters of Purkinje cell dendrites into the expression for $\langle d_d \rangle$ in *Eq. 32*. First, experimental measurements for the specific membrane resistance R_m and the intracellular resistivity R_i (Roth and Häusser 2001) yield $\beta = [R_m/(4R_i)]^{1/2} = 2 \times 10^3\ \mu m^{1/2}$. Next, by substituting other anatomical parameters, such as $C = 10^5$, $\langle d_d \rangle = 1.5\ \mu m$, $s = 1.4\ \mu m$ (Napper and Harvey 1988b), and $d_a = 0.2\ \mu m$ (Napper and Harvey 1988a), into *Eq. 32*, we find $\alpha \sim 4\ \mu m^2$.

Experimental tests needed to differentiate between the two cost functions

The two models make the following predictions about dendritic diameters. Testing these predictions experimentally could help determine which model is correct.

1) The two models predict different branching laws for dendritic diameters at a bifurcation point (Fig. 6). By combining data from different bifurcation points on a scatterplot d_2/d_0 versus d_1/d_0 and fitting it by the function $(d_1/d_0)^\eta + (d_2/d_0)^\eta = 1$ (Chklovskii and Stepanyants 2003), one could determine the value of exponent η. The transport model predicts $\eta = 2$, whereas the signal attenuation model predicts $\eta = 3/2$. To distinguish between the two models, one would need highly precise measurements of diameters, which may become available soon from electron microscopic reconstructions. The difference between the predictions of the two models is greatest for symmetric bifurcations (Wittenberg and Wang 2007), where daughter branches have approximately the same caliber.

It would be interesting to see whether our theory is applicable to highly asymmetric branching points, where one daughter branch is considerably thinner and shorter than the other. For the shorter branch, the approximation that the attenuation cost is proportional to the electrotonic length may break down due to the smaller space constant and the sealed-end boundary effect on the current flow. Yet, the dependence of diameters on the exponent in the branching law is weak in this case, making it hard to distinguish between different cost functions. In addition, one could test the transport model by counting the number of microtubules in the mother branch and comparing it with the sum of the microtubules in the daughter branches.

2) The two models make different predictions about the dependence of the mean dendritic diameter on the path length and the dependence of the diameter of stem segments near the soma, d_s, on the total dendritic length. Given that the total dendritic length is proportional to the total number of synapses on the arbor, the transport model predicts $\langle d_d^2 \rangle \sim \ell$ and $\sum d_s^2 \sim L$, where we sum over different stem segments. At the same time, the signal attenuation model predicts $\langle d_d \rangle \sim \ell^{2/3}$ and $\sum d_s^{3/2} \sim L$.

To distinguish between the scaling laws derived from the two models, one could take measurements on dendrites that belong to the same neuronal class but vary in arbor size and total dendritic length. For example, one may measure pyramidal neurons in different primate cortical areas, where dendritic arbor size and total dendritic length vary (Elston et al. 1999).

Extension of the theory to other cell types

Although we were able to rationalize the shape of Purkinje cell dendrites, neuronal arbor shape varies among cell classes.

In particular, cortical pyramidal cell dendrites have 3D shape and are sparser than Purkinje cell dendrites, suggesting that they do not achieve the minimum dendritic cost. How can we understand the shape of such dendrites?

One difference between the Purkinje cells in the cerebellum and the pyramidal cells in the cortex is the geometry of axons representing their dominant input. Unlike parallel fibers in the cerebellum, cortical axons run in different directions. Thus a flat dendritic arbor can effectively capture only those axons that are oriented near orthogonally to the dendritic plane. This could explain the 3D shape of pyramidal cells by the different shape of cortical axons. Whether the sparseness of pyramidal cells can be due to the shape of corresponding axons or requires the introduction of another principle will be addressed elsewhere.

Developmental mechanisms of arbor growth

Because our work is based on evolutionary fitness optimization, it does not answer the question how neurons achieve observed shape in the course of development. This question is addressed by a complementary approach—simulation of neuronal arbor growth (Samsonovich and Ascoli 2005; van Ooyen and Willshaw 2000; van Pelt and Uylings 2002; van Pelt et al. 1997). In particular, Sugimura et al. (2007) recently proposed a mechanistic model of Purkinje arbor growth, in which two types of hypothetical molecules—an activator and a suppressor—control dendritic growth. Arbor growth is catalyzed by the activator and inhibited by the activator-induced suppressor. The development of arbor shape is determined by a set of differential equations, the solution of which could form branching patterns uniformly covering 2D dendritic territory, just like Purkinje cell dendrites. This work provides a possible answer of how to build a compact 2D dendritic arbor, although it remains to be seen whether the simulated dendrites would have the same mesh size as that of the Purkinje cell dendrites.

ACKNOWLEDGMENTS

We thank A. Stepanyants, J. Snider, and Y. Mishchenko for a critical reading of the manuscript and many valuable suggestions and two anonymous reviewers for helpful comments.

Present address of Q. Wen and D. B. Chklovskii: Janelia Farm Research Campus, Howard Hughes Medical Institute, 19700 Helix Drive, Asburn, VA 20147.

GRANTS

This work was supported by the Swartz Foundation, the Klingenstein Foundation, and National Institute of Mental Health Grant MH-69838.

REFERENCES

Agmon-Snir H, Carr CE, Rinzel J. The role of dendrites in auditory coincidence detection. *Nature* 393: 268–272, 1998.

Attwell D, Laughlin SB. An energy budget for signaling in the grey matter of the brain. *J Cereb Blood Flow Metab* 21: 1133–1145, 2001.

Burke RE, Marks WB, Ulfhake B. A parsimonious description of motoneuron dendritic morphology using computer simulation. *J Neurosci* 12: 2403–2416, 1992.

Chklovskii DB. Synaptic connectivity and neuronal morphology: two sides of the same coin. *Neuron* 43: 609–617, 2004.

Chklovskii DB, Schikorski T, Stevens CF. Wiring optimization in cortical circuits. *Neuron* 34: 341–347, 2002.

Chklovskii DB, Stepanyants A. Power-law for axon diameters at branch point (Abstract). *BMC Neurosci* 4: 18, 2003.

Cline HT. Dendritic arbor development and synaptogenesis. *Curr Opin Neurobiol* 11: 118–126, 2001.

Cuntz H, Borst A, Segev I. Optimization principles of dendritic structure. *Theor Biol Med Model* 4: 21, 2007.

Debanne D. Information processing in the axon. *Nat Rev Neurosci* 5: 304–316, 2004.

Elston GN, Tweedale R, Rosa MG. Cellular heterogeneity in cerebral cortex: a study of the morphology of pyramidal neurones in visual areas of the marmoset monkey. *J Comp Neurol* 415: 33–51, 1999.

Fiala JC, Harris KM. Dendritic structure. In: *Dendrites*, edited by Stuart G, Spruston N, Häusser M. New York: Oxford Univ. Press, 1999, p. 1–34.

Grossman Y, Parnas I, Spira ME. Differential conduction block in branches of a bifurcating axon. *J Physiol* 295: 283–305, 1979a.

Grossman Y, Parnas I, Spira ME. Mechanisms involved in differential conduction of potentials at high frequency in a branching axon. *J Physiol* 295: 307–322, 1979b.

Gundappa-Sulur G, De Schutter E, Bower JM. Ascending granule cell axon: an important component of cerebellar cortical circuitry. *J Comp Neurol* 408: 580–596, 1999.

Hillman D. Neuronal shape parameters and substructures as a basis of neuronal form. In: *Neurosciences: Fourth Study Program.* Cambridge, MA: MIT Press, 1979, p. 477–498.

Hsu A, Tsukamoto Y, Smith RG, Sterling P. Functional architecture of primate cone and rod axons. *Vision Res* 38: 2539–2549, 1998.

Jan YN, Jan LY. The control of dendrite development. *Neuron* 40: 229–242, 2003.

Koch C. *Biophysics of Computation: Information Processing in Single Neurons.* New York: Oxford Univ. Press, 1999, p. xxiii, 562.

Koch C, Poggio T, Torre V. Retinal ganglion cells: a functional interpretation of dendritic morphology. *Philos Trans R Soc Lond B Biol Sci* 298: 227–263, 1982.

Lennie P. The cost of cortical computation. *Curr Biol* 13: 493–497, 2003.

Llinás RR, Walton KD, Lang EJ. Cerebellum. In: *The Synaptic Organization of the Brain*, edited by Shepherd GM. New York: Oxford Univ. Press, 2004, p. 271–309.

London M, Häusser M. Dendritic computation. *Annu Rev Neurosci* 28: 503–532, 2005.

Mainen ZF, Sejnowski TJ. Influence of dendritic structure on firing pattern in model neocortical neurons. *Nature* 382: 363–366, 1996.

Manor Y, Koch C, Segev I. Effect of geometrical irregularities on propagation delay in axonal trees. *Biophys J* 60: 1424–1437, 1991.

Martone ME, Zhang S, Gupta A, Qian X, He H, Price DL, Wong M, Santini S, Ellisman MH. The cell-centered database: a database for multiscale structural and protein localization data from light and electron microscopy. *Neuroinformatics* 1: 379–395, 2003.

Murre JM, Sturdy DP. The connectivity of the brain: multi-level quantitative analysis. *Biol Cybern* 73: 529–545, 1995.

Napper RM, Harvey RJ. Number of parallel fiber synapses on an individual Purkinje cell in the cerebellum of the rat. *J Comp Neurol* 274: 168–177, 1988a.

Napper RM, Harvey RJ. Quantitative study of the Purkinje cell dendritic spines in the rat cerebellum. *J Comp Neurol* 274: 158–167, 1988b.

Nevian T, Larkum ME, Polsky A, Schiller J. Properties of basal dendrites of layer 5 pyramidal neurons: a direct patch-clamp recording study. *Nat Neurosci* 10: 206–214, 2007.

Poirazi P, Mel BW. Impact of active dendrites and structural plasticity on the memory capacity of neural tissue. *Neuron* 29: 779–796, 2001.

Purves D. *Body and Brain: A Trophic Theory of Neural Connections.* Cambridge, MA: Harvard Univ. Press, 1988.

Rall W. Branching dendritic trees and motoneuron membrane resistivity. *Exp Neurol* 1: 491–527, 1959.

Ramón y Cajal S. *Textura del Sistema Nervioso del Hombre y de los Vertebrados* (*Texture of the Nervous System of Man and the Vertebrates*). New York: Springer-Verlag, 1899.

Rapp M, Segev I, Yarom Y. Physiology, morphology and detailed passive models of guinea-pig cerebellar Purkinje cells. *J Physiol* 474: 101–118, 1994.

Roth A, Häusser M. Compartmental models of rat cerebellar Purkinje cells based on simultaneous somatic and dendritic patch-clamp recordings. *J Physiol* 535: 445–472, 2001.

Samsonovich AV, Ascoli GA. Statistical morphological analysis of hippocampal principal neurons indicates cell-specific repulsion of dendrites from their own cell. *J Neurosci Res* 71: 173–187, 2003.

Samsonovich AV, Ascoli GA. Statistical determinants of dendritic morphology in hippocampal pyramidal neurons: a hidden Markov model. *Hippocampus* 15: 166–183, 2005.

Scott EK, Luo L. How do dendrites take their shape? *Nat Neurosci* 4: 359–365, 2001.

Stepanyants A, Hof PR, Chklovskii DB. Geometry and structural plasticity of synaptic connectivity. *Neuron* 34: 275–288, 2002.

Sugimura K, Shimono K, Uemura T, Mochizuki A. Self-organizing mechanism for development of space-filling neuronal dendrites. *PLoS Comput Biol* 3: e212, 2007.

Trachtenberg JT, Chen BE, Knott GW, Feng G, Sanes JR, Welker E, Svoboda K. Long-term in vivo imaging of experience-dependent synaptic plasticity in adult cortex. *Nature* 420: 788–794, 2002.

van Ooyen A, Willshaw DJ. Development of nerve connections under the control of neurotrophic factors: parallels with consumer-resource systems in population biology. *J Theor Biol* 206: 195–210, 2000.

van Pelt J, Dityatev AE, Uylings HB. Natural variability in the number of dendritic segments: model-based inferences about branching during neurite outgrowth. *J Comp Neurol* 387: 325–340, 1997.

van Pelt J, Uylings HB. Branching rates and growth functions in the outgrowth of dendritic branching patterns. *Network* 13: 261–281, 2002.

Vetter P, Roth A, Häusser M. Propagation of action potentials in dendrites depends on dendritic morphology. *J Neurophysiol* 85: 926–937, 2001.

Wen Q, Chklovskii DB. Segregation of the brain into gray and white matter: a design minimizing conduction delays. *PLoS Comput Biol* 1: e78, 2005.

Whitford KL, Dijkhuizen P, Polleux F, Ghosh A. Molecular control of cortical dendrite development. *Annu Rev Neurosci* 25: 127–149, 2002.

Wittenberg GM, Wang SS-H. Evolution and scaling of dendrites. In: *Dendrites* (2nd ed.), edited by Häusser M, Spruston N, Stuart G. New York: Oxford Univ. Press, 2007, p. 43–67.

Zador AM, Agmon-Snir H, Segev I. The morphoelectrotonic transform: a graphical approach to dendritic function. *J Neurosci* 15: 1669–1682, 1995.